Use of Alternating Current Impedance Method in Diagnosing Electrode Kinetics of $[Fe(CN)_6]^{4-/3-}$ Complex Confined to Protonated Poly(4-vinylpyridine) Film on Graphite Surfaces

Takeo OHSAKA, Toru USHIROGOUCHI, and Noboru OYAMA*
Department of Applied Chemistry for Resources, Tokyo University of Agriculture and Technology, Koganei, Tokyo 184
(Received June 26, 1985)

A "heterogeneous" electron-transfer process of $[Fe(CN)_6]^{4-/3-}$ redox couple, which was confined electrostatically to the protonated poly(4-vinylpyridine) (PVP) film, at basal-plane pyrolytic graphite (BPG) electrode/PVP film interfaces and a "homogeneous" charge-transport process within the PVP film were examined by alternating current (ac) impedance method. The obtained impedance loci were found to correspond to those expected for the electrochemical impedance expressed by "Randles's equivalent circuit." The relevant kinetic parameters (*i.e.*, the standard rate constant, $k°$ and the cathodic transfer coefficient, α) of the electrode reaction, the apparent diffusion coefficients, D_{app}, for the "homogeneous" charge-transport within the film, the double-layer capacity, C_{dl} and the solution resistance, R_{soln} were determined at various concentrations of $[Fe(CN)_6]^{3-}$ in PVP coatings. The obtained D_{app}, $k°$, and α values were compared with those recently obtained by normal pulse voltammetry. In addition, an equivalent circuit model is given for the impedance obtained for the redox reaction on a BPG electrode coated with a protonated PVP confining $[Fe(CN)_6]^{4-/3-}$ couple.

Recently, there has been much attention focused on the physical, electrochemical, photoelectrochemical, and other kinds of behavior of "polymer-coated electrode."[1] A key question concerning the behavior involves the kinetics of two distinct charge (ion or electron)-transfer processes: One is the "homogeneous" charge-transfer process within polymer coatings and another is the "heterogeneous" electron-transfer process between electrode and redox species (or sites) confined to polymeric domains. In a series of recent papers,[2-9] we have reported the kinetic study of these both charge-transfer processes for various polymer-coated electrode systems by means of a normal pulse voltammetry (NPV). They involve the $[Mo(CN)_8]^{4-/3-}$, $[Fe(CN)_6]^{4-/3-}$, $[W(CN)_8]^{4-/3-}$, and $[IrCl_6]^{3-/2-}$-protonated poly(4-vinylpyridine) (PVP) systems,[2-5] the $[Fe(CN)_5]^{3-/2-}$–PVP system,[4] the $[Fe(CN)_6]^{4-/3-}$–poly(*N*,*N*-dimethylaniline) system,[8] the $MV^{2+/+}$-Nafion® system (MV^{2+}: *N*,*N*′-dimethyl-4,4′-bipyridinium)[6] the poly(xylylviologen)-poly(*p*-styrenesulfonate) (PSS) system,[6] and the poly(methylviologen) (PMV), PMV–Nafion and PMV–PSS systems.[6,7,9] Some interesting results were obtained: (i) the values of the standard rate constant ($k°$) of the heterogeneous electron-transfer process and the apparent diffusion coefficient (D_{app}) for the diffusion-like charge-transport process within the polymer films are smaller than those for the corresponding solution-phase redox species, (ii) the $k°$ and D_{app} depend on the concentration (c_p) of the redox species (or site) confined to the polymer, (iii) the $k°$ and D_{app} change with the polymers confining the redox species (or site) and/or the supporting electrolytes, (iv) the transfer coefficient (α) of the heterogeneous electron-transfer process changes with c_p in some cases, and (v) there are linear relationships between log $k°$ and log D_{app}. These results, which have not been completely explained yet, are of specific interest to this work.

In the present study, in order to obtain further information about the above-mentioned points, we examine the kinetics of the heterogeneous electron-transfer process of the $[Fe(CN)_6]^{4-/3-}$ couple confined to the protonated PVP coating on a pyrolytic graphite electrode as well as the homogeneous charge-transport process within the coating by means of ac impedance method, which has been recently increasingly gaining interest for characterization of the polymer films deposited on electrode surfaces (*e.g.*, glow-discharge polymer films prepared on Pt electrode from 4-vinylpyridine,[10] electropolymerized polypyrrole film,[11-13] polyacetylene film[14]). The data obtained are compared with those previously obtained by NPV. In addition, an equivalent circuit model for the impedance obtained with the redox reaction on a BPG electrode which is coated with a protonated PVP confining $[Fe(CN)_6]^{4-/3-}$ couple is represented.

Experimental

Materials. The basal-plane pyrolytic graphite (BPG) (Union Carbide Co.) disk electrodes (area: 0.17 cm^2) were prepared and mounted into glass tube with heat-shrinkable polyolefin tube as previously described.[15] Poly(4-vinylpyridine) (PVP) (Borden Inc., Philadelphia, Pa) was recrystallized from methanol–diethyl ether. Its average molecular weight was 7.4×10^5. Potassium hexacyanoferrate(III), $K_3[Fe(CN)_6]$, was of reagent grade (Merck). Aqueous solutions were prepared from doubly distilled water. The supporting electrolyte solution was 0.2 M (1 M=1 mol dm^{-3}) CF_3COONa (Aldrich) adjusted to pH 1.5 with CF_3COOH. Other chemicals were reagent grade and were used as received.

Apparatus and Procedures. The electrochemical measurement was made with a conventional potentiostatic device with three electrodes. The working electrodes were BPG disk electrodes coated with PVP films to which

$[Fe(CN)_6]^{3-}$ ions were confined electrostatically at various concentrations.[2-8, 15] The counter electrode was a spiral platinum wire with a surface area of *ca.* 20 cm^2. The reference electrode was a sodium chloride saturated calomel electrode (SSCE). All potentials were measured and are reported with respect to SSCE. The working electrode was potentiostated at a given dc potential and then a sinusoidal perturbation signal with an amplitude (ΔE) of 5.0 mV was superimposed onto the dc potential.

The ac impedance measurements were performed with a Frequency Response Analyzer (Solartron Model 1250) and a Potentiostat/Galvanostat 2000 (Toho Technical Research, Tokyo) equipped with GPIB interface. Measurements were carried out in the potentiostatic mode. The impedance diagrams were plotted in the frequency range from 1 Hz to 65 kHz at 10 points per frequency decade. The impedance data were transferred to the laboratory's minicomputer (NEC, PC-9801E) where calculation and tabulation were performed, and then graphically presented on a plotter (Hewlett Packard 7470A) in the form of complex impedance plane plots of Z'' *vs.* Z' and/or in the form of complex admittance plane plots of Y''/ω *vs.* Y'/ω, where Z and Y are the complex impedance and the complex admittance, respectively and superscripts $'$ and $''$ on Z and Y denote in-phase and quadrature (*i.e.*, 90° out-of-phase) components, and ω is the angular frequency. The tabulated data were stored on a computer disk file ready for further analysis.

Coatings of PVP were prepared by micropipetting 1 to 10 µl aliquots of a methanolic stock solution of PVP (0.5%) onto freshly cleaved BPG electrodes and allowing the solvent to evaporate.[2-5, 15, 16] Electrostatic binding of $[Fe(CN)_6]^{3-}$ ions to the protonated PVP coatings resulted from exposure of the coated electrodes to 0.2—10 mM solutions of $K_3[Fe(CN)_6]$ in a 0.2 M CF_3COONa solution (pH 1.5) for periods of 1 to 30 min depending on the desired quantity of incorporated $[Fe(CN)_6]^{3-}$. The quantities (coverage values) of $[Fe(CN)_6]^{3-}$ incorporated into the protonated PVP coatings were determined by transferring the electrodes into solutions containing only supporting electrolyte (0.2 M CF_3COONa-CF_3COOH (pH 1.5)) and integrating the current-time curves obtained when the potential was stepped to a value well beyond the voltammetric peak potential and held there until the rate of charge accumulation decreased to background levels. The coverage value was obtained in units of mol cm^{-2} and then the molar concentration (in units of mol cm^{-3}) was calculated by using the thickness of the PVP film estimated by assuming that the density of the wet PVP is 0.65 g cm^{-3}.[16]

Nitrogen gas was passed through the solutions to remove the dissolved oxygen before the measurements and over the solutions during the measurements. Experiments were conducted at 25 °C.

Results and Discussion

Impedance Measurements of the $[Fe(CN)_6]^{4-/3-}$-protonated PVP System. Figure 1 shows the typical cyclic voltammogram for the $[Fe(CN)_6]^{4-/3-}$ couple confined to the protonated PVP coating on a BPG electrode in a 0.2 M CF_3COONa solution (pH 1.5). The wave shape is similar to that for the solution-phase $[Fe(CN)_6]^{4-/3-}$ couple at a bare electrode, that is, the wave is diffusion-like, with broad peaks and a diffusion tail. The peak height and wave shape of the cyclic voltammogram remained substantially unchanged after 30 min when the electrode potential was scanned between −0.2 and 0.8 V *vs.* SSCE at 100 mV s^{-1}. The survival of the electrostatically bound $[Fe(CN)_6]^{4-/3-}$ couple for such long periods allowed us to carry out ac impedance measurements of this system.

In Fig. 2 are shown typical Cole-Cole plots (*i.e.*, plots of the quadrature component of the ac impedance *vs.* its real component) for the redox reaction of the $[Fe(CN)_6]^{4-/3-}$ couple confined to the protonated PVP film on BPG electrodes. The data in Fig. 2 show the complex plane impedance plots for the redox reaction of the $[Fe(CN)_6]^{4-/3-}$ couple at each formal redox potential. The formal redox potential for the $[Fe(CN)_6]^{4-/3-}$ confined to the protonated PVP film, which was estimated as the average of the anodic and cathodic peak potentials of the cyclic voltammograms (such as those shown in Fig. 1) for the redox reaction of the $[Fe(CN)_6]^{4-/3-}$ couple confined to the protonated PVP film, changed with the $[Fe(CN)_6]^{3-}$ concentration. Both of these curves were obtained at each formal redox potential, curve A taken at 0.275 V *vs.* SSCE and curve B at 0.265 V *vs.* SSCE. It can be seen that the impedance loci of these curves correspond to those expected for the electrochemical impedance represented by the well-known "Randles's equivalent circuit" (shown in Fig. 3).[17] The double-layer capacity C_{dl}, in parallel with the electron-transfer resistance R_{et}, gives rise to the circular part of the diagram (line I in Fig. 2). A straight line of unity slope (line II) corresponds to

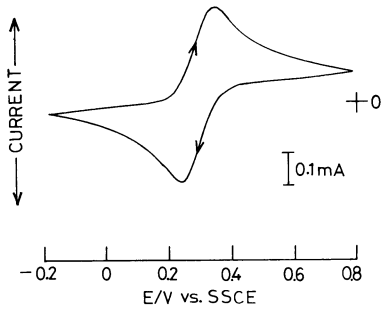

Fig. 1. A typical cyclic voltammogram for the oxidation-reduction of the $[Fe(CN)_6]^{4-/3-}$ redox couple confined to the protonated PVP film on a BPG electrode in a 0.2 M CF_3COONa solution (pH 1.5). Surface concentration of pyridine as PVP, Γ_{PVP}: 4.6×10^{-7} mol cm^{-2}. The concentration of $[Fe(CN)_6]^{3-}$ confined to protonated PVP film (thickness: 7.1×10^{-5} cm): 5.5×10^{-4} mol cm^{-3}. Scan rate: 100 mVs^{-1}.

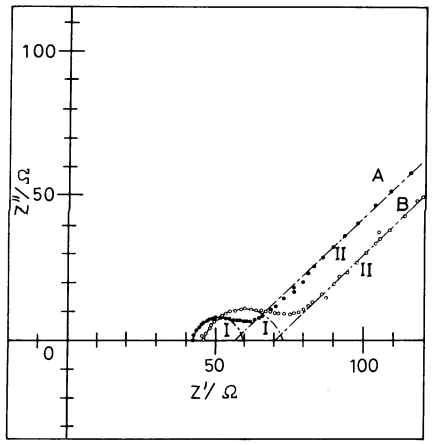

Fig. 2. Typical Cole-Cole plots for the redox reaction of the $[Fe(CN)_6]^{4-/3-}$ couple confined to the protonated PVP film on BPG electrodes in a 0.2 M CF_3COONa solution (pH 1.5). In both cases (A and B), the thicknesses of the PVP films were 8.7×10^{-5} cm and the surface concentration (Γ_{PVP}) of the pyridine site of PVP was 5.6×10^{-7} mol cm^{-2}. The concentrations (c_p) of $[Fe(CN)_6]^{3-}$ in PVP films were (A) 1.1×10^{-3} and (B) 4.1×10^{-4} mol cm^{-3}. The molar ratios of incorporated $[Fe(CN)_6]^{3-}$ to protonated pyridine site of PVP ($\Gamma_{[Fe(CN)_6]^{3-}}/\Gamma_{PVP}$) were (A) 0.17 and (B) 0.069. The dc potentails were set at (A) 0.275 and (B) 0.265 V *vs.* SSCE which were formal redox potentials in cases A and B. The amplitude of an imposed ac voltage was 5.0 mV.

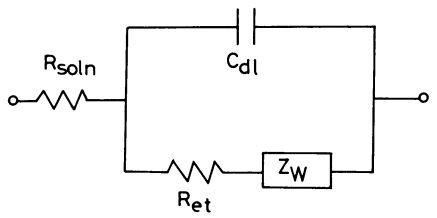

Fig. 3. Randles's equivalent circuit.
R_{soln} denotes solution resistance, R_{et} electron-transfer resistance, C_{dl} double-layer capacity, and Z_w Warburg diffusional impedance.

the Warburg diffusional impedance Z_w which arises as a consequence of diffusional polarization resulting from an imposed ac voltage.[18] Strictly speaking, the impedance plots shown in Fig. 2 are not perfectly semicircles. The center of the semicircle lies slightly below the real axis. This problem will be in detail discussed in the next section. As a first approximation, the impedance loci obtained may be expressed by the Randles's equivalent circuit. Thus, the kinetic parameters concerning the heterogeneous electron-transfer process and homogeneous charge-transport process (*i.e.*, the standard rate constant k° and the transfer coefficient α of heterogeneous electron-transfer and the apparent diffusion coefficient D_{app} for the charge-transport within polymer coatings) are estimated on the basis of the conventional analysis[18,19] of the complex impedance plane plots such as those shown in Fig. 2. According to the Randles's equivalent circuit shown in Fig. 3, the diameter of the semicircle equals the heterogeneous electron-transfer resistance R_{et}, while the double-layer capacity C_{dl} can be calculated from the angular frequency ω_{max} which corresponds to the maximum of the semicircle by using the relation $\omega_{max}R_{et}C_{dl}=1$ with $\omega=2\pi f$. From the R_{et} obtained, the k° can be calculated. The solution resistance R_{soln} is obtained from the high-frequency intercept with the real axis. Further, the diffusion coefficient can be obtained from the intercept of the line II with the real axis by knowing R_{soln} and C_{dl} and assuming that the diffusion coefficients for $[Fe(CN)_6]^{4-}$ and $[Fe(CN)_6]^{3-}$ are the same. It is apparent from curves A and B that the R_{soln} and R_{et} vary with the concentration of $[Fe(CN)_6]^{3-}$ in the PVP coatings. The values of R_{soln}, D_{app}, k°, and C_{dl} were estimated by the above-mentioned procedures and the data obtained are summarized below. The values of α were estimated from the analysis of the phase angle ϕ as mentioned below. By the similar analysis of ϕ, the k° values were also obtained.

The phase angle ϕ for the simple electrode process, $Ox+ne\rightleftarrows Red$, which is of great interest as a source of kinetic information about the heterogeneous electron-transfer reaction, can be expressed as follows:[18,19]

$$\cot\phi = 1 + \frac{(2D_{Ox}^{1-\alpha}D_{Red}^{\alpha}\omega)^{1/2}}{k^\circ}\cdot\left[\frac{1}{e^{(1-\alpha)\xi}(1+e^{-\xi})}\right] \quad (1)$$

with

$$\xi = \frac{nF}{RT}(E_{dc}-E_{1/2}), \quad (2)$$

where D_{Ox} and D_{Red} are the diffusion coefficients of Ox and Red, respectively, α is the cathodic transfer coefficient, E_{dc} is the applied dc potential, $E_{1/2}$ is the reversible half-wave potential of the Ox/Red couple, n is the number of electrons involved in the heterogeneous electron-transfer reaction, F is the Faraday constant, R is the gas constant, and T is the absolute temperature. The bracketed factor indicates that cot ϕ depends on the dc potential. That is, at large negative value of ξ, cot ϕ is close to 1 (*i.e.*, when $\xi\rightarrow-\infty$, cot $\phi\rightarrow1$). As ξ increases, cot ϕ increases and passes the maximum point. With further increase in ξ, cot ϕ decreases and at large positive value of ξ cot ϕ approaches to 1 (*i.e.*, when $\xi\rightarrow+\infty$, cot $\phi\rightarrow1$). The dc potential at which cot ϕ is a maximum is given by

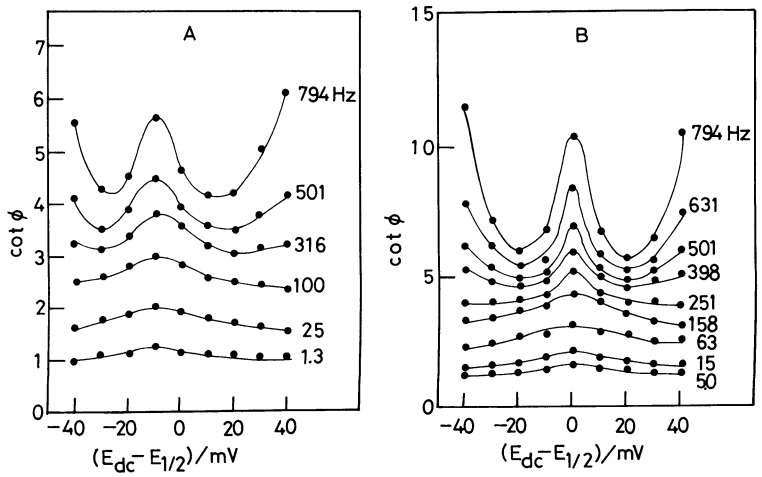

Fig. 4. Dependence of cot ϕ on E_{dc}.
The plots A and B correspond to cases A and B, respectively, shown in Fig. 2. The experimental conditions are the same as in Fig. 2. The numbers on respective plots indicate angular frequencies.

$$E_{dc} = E_{1/2} + \frac{RT}{nF} \ln \frac{\alpha}{1-\alpha}. \quad (3)$$

Thus, this maximum point is independent of nearly all experimental variables, for example, the amplitude of the applied ac voltage ΔE, the electrode area A and the angular frequency ω. The difference between $E_{1/2}$ and the potential of maximum cot ϕ provides transfer coefficient α. A typical example of such behavior is shown in Fig. 4. Note that the potential of maximum cot ϕ is independent of frequency, as predicted above. In the case of Fig. 4B (corresponding to curve B (c_p: 4.1×10^{-4} mol cm^{-3}) in Fig. 2), the maximum point is at $E_{dc}-E_{1/2}=0$ and thus α is 0.5. Similarly, in the case of Fig. 4A which corresponds to curve A (c_p: 1.1×10^{-3} mol cm^{-3}) in Fig. 2, the α value is estimated as 0.41. The dependence of α on c_p has been previously observed for the same redox system[4] as that examined here and for the other redox polymer-coated electrode systems.[2,3,5-9] The previous studies were conducted by NPV. The present data of α were in fair agreement with those obtained by NPV.

Further, it is also apparent from Fig. 4 that at higher frequencies, cot ϕ tends to increase as the value of $E_{dc}-E_{1/2}$ becomes larger. The reason for this behavior is not clear, but this may be probably due to the variation of C_{dl} in the dc potential region examined (see Fig. 7).

As can be seen from Eq. 1, plots of cot ϕ *vs.* $\omega^{1/2}$ yield k°, once α is known from the potential of maximum cot ϕ and the diffusion coefficients are known from the intercept of line II with the real axis or other measurements. Especially, at $E_{dc}=E_{1/2}$, $\xi=0$, and thus Eq. 1 can be reduced to Eq. 4

Typical examples of $[\cot\phi]_{E_{1/2}}$ *vs.* $\omega^{1/2}$ plots are shown in Fig. 5. As expected from Eq. 4, the straight

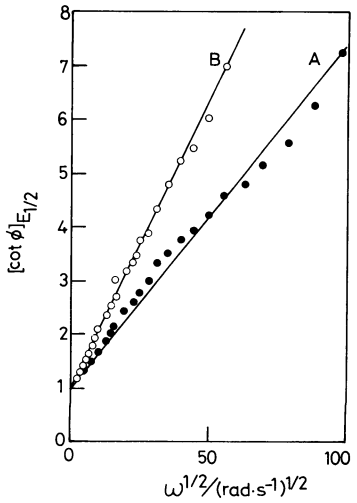

Fig. 5. Plots of $[\cot\phi]_{E_{1/2}}$ *vs.* $\omega^{1/2}$.
The plots A and B correspond to cases A and B, respectively, shown in Fig. 2. The experimental conditions and the symbols are the same as in Fig. 2. [cot $\phi]_{E_{1/2}}$ indicates cot ϕ at $E=E_{1/2}$.

$$[\cot\phi]_{E_{1/2}} = 1 + \left(\frac{D_{Ox}^{1-\alpha} D_{Red}^{\alpha}}{2}\right)^{1/2} \cdot \frac{\omega^{1/2}}{k^\circ}. \quad (4)$$

lines with the intercept of 1 on the ordinate can be obtained. The different slopes of these straight lines are ascribable to the different k°'s and/or D_{app}'s.

The data obtained for k° and D_{app} at the different concentrations of $[Fe(CN)_6]^{3-}$ in PVP coating are summarized in Fig. 6, where the data obtained by NPV are also shown for comparison. It can be seen from this figure that the k° values obtained from the R_{et} values by ac impedance method are almost equal to those obtained by NPV, while the D_{app} values are by about 1 to 2 orders of magnitude smaller than those obtained by NPV. The observed differences

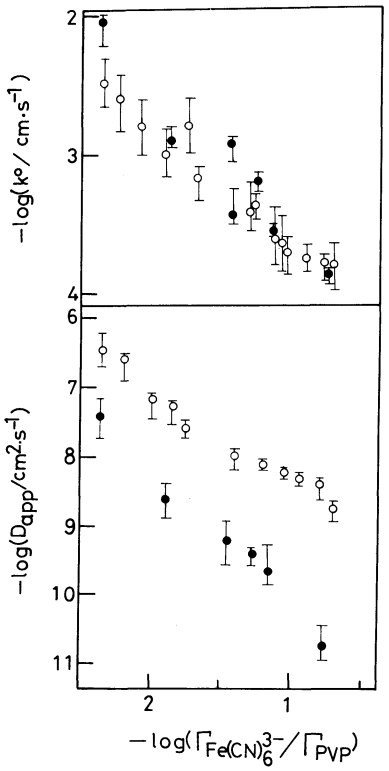

Fig. 6. Plots of the logarithms of D_{app} and k° *vs.* the logarithm of the molar ratio of incorporated $[Fe(CN)_6]^{3-}$ to the protonated pyridine site of PVP, $\Gamma_{[Fe(CN)_6]^{3-}}/\Gamma_{PVP}$. The thicknesses of the PVP films were 8.7×10^{-5} cm. Γ_{PVP}: 5.6×10^{-7} mol cm^{-2}. Supporting electrolyte: 0.2 M CF_3COONa–CF_3COOH (pH 1.5). The closed and open circles indicate the data obtained by ac impedance method and normal pulse voltammetry, respectively.

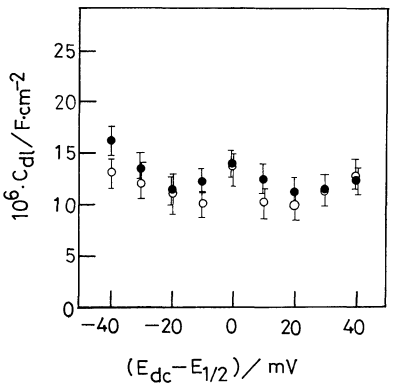

Fig. 7. Dependence of C_{dl} on $(E_{dc}-E_{1/2})$. c_p: (●) 1.1×10^{-3} and (○) 4.1×10^{-4} mol cm^{-3}. Other experimental conditions are the same as in Fig. 6.

between the D_{app} values obtained by the two methods seem not to be due to only the errors in the D_{app} estimation by ac impedance method, although the determination of D_{app} by ac impedance method is less accurate than the k° estimation. At the present stage,

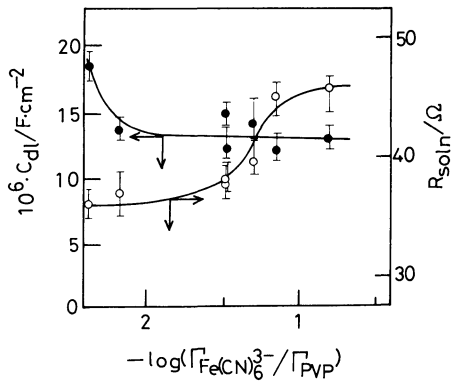

Fig. 8. Dependences of C_{dl} and R_{soln} on $-\log(\Gamma_{[Fe(CN)_6]^{3-}}/\Gamma_{PVP})$. The experimental conditions are the same as in Fig. 6. The values of C_{dl} and R_{soln} were obtained from the complex impedance loci such as those shown in Fig. 2 which were measured at the respective formal redox potentials, depending on $\Gamma_{[Fe(CN)_6]^{3-}}/\Gamma_{PVP}$.

we have no reasonable explanation for such differences in D_{app}'s, but this may be considered to be ascribed to the different time windows of these two methods in the D_{app} estimation, *i.e.*, the time window of ac impedance method is *ca.* one order of magnitude shorter than that of NPV. It is also apparent that the k° and D_{app} depend on the concentration (c_p) of $[Fe(CN)_6]^{3-}$ in polymer coatings, irrespective of the methods used. Such concentration dependences of k° and D_{app} may be understood by the same idea as that used previously:[2-6] As c_p increases, the extent of electrostatic cross-linking of PVP polymer by electrostatic force between multiply-charged anion (*i.e.*, $[Fe(CN)_6]^{3-}$) and positively charged protonated pyridine sites of PVP becomes higher and as a result the physical motion of $[Fe(CN)_6]^{3-}$ and/or supporting electrolytic ions through the film becomes more difficult.

Figure 7 shows the dependence of the double-layer capacity C_{dl} on the dc potential E_{dc}. It is obvious that C_{dl} depends on E_{dc} in the examined range of the potential. Such dependence of C_{dl} on E_{dc} seems to be almost the same irrespective of c_p. The values of C_{dl} are almost the same as those obtained with a bare BPG electrode in the same supporting electrolytic solution as that used here. Figure 8 shows the dependence of C_{dl} and the solution resistance (R_{soln}) upon c_p. The C_{dl} tends to decrease with an increase in c_p, while the R_{soln} increases with increasing c_p.

Equivalent Circuit Model for the Redox Reaction of $[Fe(CN)_6]^{4-/3-}$ Couple Confined to the Protonated PVP Coatings on BPG Electrodes. In the previous section, the impedance loci for the redox reaction of $[Fe(CN)_6]^{4-/3-}$ couple confined to the PVP coating on BPG electrodes were analyzed by assuming that the equivalent circuit for this redox reaction system can be expressed by the Randles's equivalent circuit (Fig.

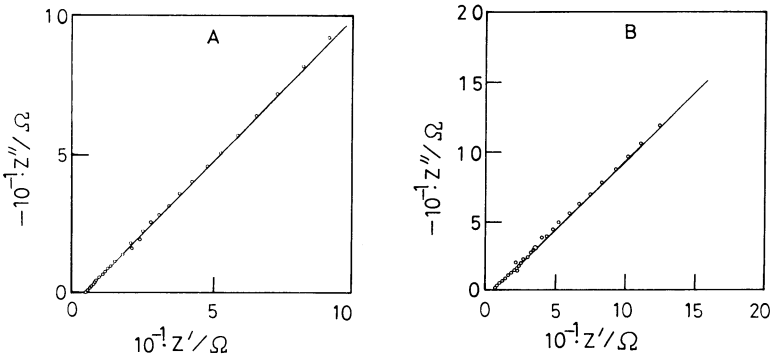

Fig. 9. The complex impedance plane plots finally obtained according to the procedure of De Levie *et al.*
The plots A and B correspond to cases A and B, respectively, shown in Fig. 2.

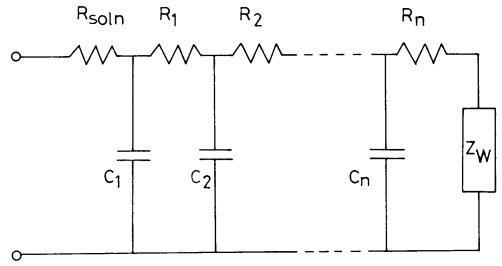

Fig. 10. The transmission line equivalent circuit obtained for the redox reaction of the $[Fe(CN)_6]^{4-/3-}$ couple confined to the protonated PVP film on BPG electrodes.
For the case A in Fig. 2, $R_{soln}=42\,\Omega$, $R_1=10\,\Omega$, $R_2=3\,\Omega$, $R_3=2\,\Omega$, $R_4=3\,\Omega$, $C_1=1.25\,\mu F$, $C_2=2\,\mu F$, $C_3=3\,\mu F$, and $C_4=6\,\mu F$, and for the case B in Fig. 2, $R_{soln}=45\,\Omega$, $R_1=14\,\Omega$, $R_2=7\,\Omega$, $R_3=5\,\Omega$, $C_1=1\,\mu F$, $C_2=1.7\,\mu F$, and $C_3=6\,\mu F$.

3). To elucidate equivalent circuit model expressing more exactly the actual redox reaction, the following procedure, originally suggested by De Levie *et al.*[20,21] for the analysis of ac impedance data, was used. The complex impedance representation such as that shown in Fig. 2 is first made and the frequency-independent resistance component R (in this case, solution resistance R_{soln}) can be obtained as an intercept on the abscissa by extrapolation of the impedance locus to infinite frequency. After subtraction of R_{soln}, the remaining impedance is transformed into an admittance, devided by ω, and the frequency-independent capacitance component C was determined as an intercept on the ordinate (*i.e.*, Y''/ω axis) by extrapolating the admittance locus to infinite frequency. A series of such procedures are repeated until the 45° straight line representing the Warburg impedance in the complex impedance plane can be obtained. The finally obtained complex plane impedance plots are shown in Fig. 9, and the equivalent circuit so obtained is shown in Fig. 10. The obtained equivalent circuit is well known as the so-called "transmission line equivalent circuit (TL equivalent circuit)."[22] The TL equivalent circuit of this type has been previously presented for the impedance for a porous electrode.[22-24] The similar equivalent circuit has been presented for electrodes where homogeneous or heterogeneous chemical processes are coupled to the heterogeneous electron-transfer step and also where adsorption of reactants or products or both occurs.[22] The obtainment of TL equivalent circuit can be considered to be due to a result of an "impedance dispersion."[25-28] This phenomenon, which is explained by the distribution of the time constants of the electrode processes, has been believed to be caused by (i) the influence of the microscopic roughness of the electrode surface, (ii) the selective adsorption phenomena, (iii) the non-uniform distribution of the current density on the surface, and so on. The same idea seems to be applicable to the present system. In order to obtain further information concerning this point, the kinetic study of electrode processes by ac impedance method is now extended to other polymer-coated electrode systems.

This work was partially supported by Grant-in-Aid for Scientific Research No. 59219008, for N. Oyama, from the Ministry of Education, Science, and Culture, Japan and the Nissan Science Foundation.

References

1) For example, R. W. Murray, "Electroanalytical Chemistry," ed by A. J. Bard, Marcel Dekker, New York (1984), Vol. 13, p. 191 and references therein.

2) N. Oyama, K. Sato, S. Yamaguchi, and H. Matsuda, *Denki Kagaku oyobi Kogyo Butsuri Kagaku*, **51**, 91 (1983).

3) K. Sato, S. Yamaguchi, H. Matsuda, T. Ohsaka, and N. Oyama, *Bull. Chem. Soc. Jpn.*, **56**, 2004 (1983).

4) N. Oyama, T. Ohsaka, M. Kaneko, K. Sato, and H. Matsuda, *J. Am. Chem. Soc.*, **105**, 6003 (1983).

5) N. Oyama, T. Ohsaka, and T. Ushirogouchi, *J. Phys. Chem.*, **88**, 5274 (1984).

6) T. Ohsaka, H. Yamamoto, M. Kaneko, A. Yamada, M. Nakamura, S. Nakamura, and N. Oyama, *Bull. Chem. Soc. Jpn.*, **57**, 1844 (1984).
7) T. Ohsaka, K. Sato, H. Matsuda, and N. Oyama, *J. Electrochem. Soc.*, in press (1985).
8) N. Oyama, T. Ohsaka, and T. Shimizu, *Anal. Chem.*, **57**, 1526 (1985).
9) N. Oyama, T. Ohsaka, H. Yamamoto, and M. Kaneko, *J. Phys. Chem.*, submitted.
10) K. Doblhofer, *Electrochim. Acta*, **25**, 871 (1980).
11) P. Burgmayer and R. W. Murray, *J. Am. Chem. Soc.*, **104**, 6139 (1982).
12) P. Burgmayer and R. W. Murray, *J. Phys. Chem.*, **88**, 2512 (1984).
13) R. A. Bull, F-R. F. Fan, and A. J. Bard, *J. Electrochem. Soc.*, **129**, 1009 (1982).
14) T. Osaka and T. Kitai, *Bull. Chem. Soc. Jpn.*, **57**, 759 (1984).
15) N. Oyama and F. C. Anson, *J. Am. Chem. Soc.*, **101**, 3450 (1979).
16) N. Oyama, S. Yamaguchi, Y. Nishiki, K. Tokuda, H. Matsuda, and F. C. Anson, *J. Electroanal. Chem.*, **139**, 371 (1982).
17) J. E. B. Randles, *Discuss. Faraday Soc.*, **1**, 11 (1947).
18) M. Sluyters-Rehbach and J. H. Sluyters, "Electroanalytical Chemistry," Vol. 4 (A. J. Bard, ed.), Marcel Dekker, New York (1970), p. 1.
19) A. J. Bard and L. R. Faulkner, "Electrochemical Methods, Fundamentals and Applications," Wiley, New York (1980), p. 316.
20) R. De Levie, J. W. Thomas, and K. M. Abbey, *J. Electroanal. Chem.*, **62**, 111 (1975).
21) R. De Levie and D. Vukadin, *J. Electroanal. Chem.*, **62**, 95 (1975).
22) E. Yeager and J. Kuta, "Physical Chemistry, An Advanced Treatise," ed by H. Eyring, Academic Press, New York, London (1970), Vol. 9A, p. 345.
23) L. E. A. Berlouis and G. J. Hills, *J. Electroanal. Chem.*, **180**, 401 (1984) and references therein.
24) R. De Levie, "Advances in Electrochemistry and Electrochemical Engineering," ed by P. Delehay and W. Tobias, Interscience, New York (1967), Vol. 6, p. 329.
25) V. Rammelt, G. Reinhard, and K. Rammelt, *J. Electroanal. Chem.*, **180**, 327 (1984) and references therein.
26) W. Scheider, *J. Phys. Chem.*, **79**, 127 (1975).
27) D. I. Leikis, E. S. Sevast'yanov, and L. L. Knots, *Russian J. Phys. Chem.*, **38**, 997 (1964).
28) R. J. Brodd, *J. Research, NBS*, **65A**, 275 (1961).